Monthly Notices of the ROYAL ASTRONOMICAL SOCIETY

MNRAS **474,** 5694–5703 (2018) doi:10.1093/mnras/stx3196
Advance Access publication 2017 December 11

Nitrogen oxide in protostellar envelopes and shocks: the ASAI survey

C. Codella,[1★] S. Viti,[2] B. Lefloch,[3] J. Holdship,[2] R. Bachiller,[4] E. Bianchi,[1,5] C. Ceccarelli,[3] C. Favre,[1] I. Jiménez-Serra,[6] L. Podio[1] and M. Tafalla[4]

[1]*INAF–Osservatorio Astrofisico di Arcetri, L.go E. Fermi 5, Firenze I-50125, Italy*
[2]*Department of Physics and Astronomy, University College London, Gower Street, London WC1E 6BT, UK*
[3]*CNRS, Institut de Planétologie et d'Astrophysique de Grenoble (IPAG), Univ. Grenoble Alpes, F-38000 Grenoble, France*
[4]*IGN, Observatorio Astronómico Nacional, Calle Alfonso XII, E-28004 Madrid, Spain*
[5]*Dipartimento di Fisica e Astronomia, Universitá degli Studi di Firenze, Via G. Sansone 1, I-50019 Sesto Fiorentino, Italy*
[6]*School of Physics and Astronomy, Queen Mary University of London, 327 Mile End Road, London E1 4NS, UK*

Accepted 2017 December 7. Received 2017 December 7; in original form 2017 July 17

ABSTRACT

The high sensitivity of the IRAM 30-m Astrochemical Surveys At IRAM (ASAI) unbiased spectral survey in the mm window allows us to detect NO emission towards both the Class I object SVS13-A and the protostellar outflow shock L1157-B1. We detect the hyperfine components of the $^2\Pi_{1/2} J = 3/2 \rightarrow 1/2$ (at 151 GHz) and the $^2\Pi_{1/2}$ $J = 5/2 \rightarrow 3/2$ (at 250 GHz) spectral pattern. The two objects show different NO profiles: (i) SVS13-A emits through narrow (1.5 km s^{-1}) lines at the systemic velocity, while (ii) L1157-B1 shows broad ($\sim$5 km s^{-1}) blueshifted emission. For SVS13-A, the analysis leads to $T_{\rm ex} \geq 4$ K, N(NO) $\leq 3 \times 10^{15}$ cm^{-2}, and indicates the association of NO with the protostellar envelope. In L1157-B1, NO is tracing the extended outflow cavity: $T_{\rm ex} \simeq$ 4–5 K, and N(NO) = 5.5 $\pm$ 1.5 $\times$ 10^{15} cm^{-2}. Using C^{18}O, ^{13}C^{18}O, C^{17}O, and ^{13}C^{17}O ASAI observations, we derive an NO fractional abundance less than $\sim 10^{-7}$ for the SVS13-A envelope, in agreement with previous measurements towards extended photodissociation regions (PDRs) and prestellar objects. Conversely, a definite X(NO) enhancement is measured towards L1157-B1, $\sim 6 \times 10^{-6}$, showing that the NO production increases in shocks. The public code UCLCHEM was used to interpret the NO observations, confirming that the abundance observed in SVS13-A can be attained in an envelope with a gas density of 10^5 cm^{-3} and a kinetic temperature of 40 K. The NO abundance in L1157-B1 is reproduced with pre-shock densities of 10^5 cm^{-3} subjected to a $\sim$45 km s^{-1} shock.

Key words: stars: formation – ISM: abundances – ISM: jets and outflows – ISM: molecules.

1 INTRODUCTION

The molecule of NO, Nitrogen Oxide, was first detected towards SgrB2 (Liszt & Turner 1978) and the molecular cloud OMC1 (Blake et al. 1986). Although it has now been detected in a variety of objects, ranging from dark clouds to hot cores, photon-dominated regions and nuclei of starburst galaxies (e.g. Gerin et al. 1992; Gerin, Viala & Casoli 1993; Nummelin et al. 2000; Halfen et al. 2001; Martin et al. 2003), it is seldom observed, possibly due to its complex hyperfine structure. Nevertheless, NO may be an important chemical tracer of the nitrogen chemistry cycle (e.g. Hily-Blant et al. 2010) as well as of the oxygen budget (Chen et al. 2014).

Although the chemistry of nitrogen-bearing species has been modelled in several environments (e.g. Flower, Pineau des Forêts & Walmsley 2006; Hily-Blant et al. 2010; Awad, Viti & Williams 2016), the total nitrogen abundance in the gas phase is still uncertain, especially in dense cores, as well as in the gas surrounding protostars. This is because much of the nitrogen is in the form of N and/or N_2, both not directly observable. Generally, NH, NH_2, and NH_3 are used as probes of the total nitrogen reservoir in dense star-forming gas. However, the abundance of these three species is highly dependent on how much nitrogen depletes on the surface of the grains and on the level of hydrogenation. In fact in some environments NO seems to be one of the most abundant N-bearing species: for example, Velilla Prieto et al. (2015) find that in circumstellar oxygen-rich envelopes NO is as high as 10^{-6} and one of the most abundant N-bearing species.

NO is key to form N_2, a molecule required to then form more complex nitrogen-bearing species (Hily-Blant et al. 2010) and harbours a simpler chemistry than other N-bearing species such as NH, NH_2, and NH_3. The most direct way to form NO is via neutral–neutral reactions between N and OH and, hence its abundance mainly depends on the amount of available nitrogen in the

★ E-mail: codella@arcetri.astro.it

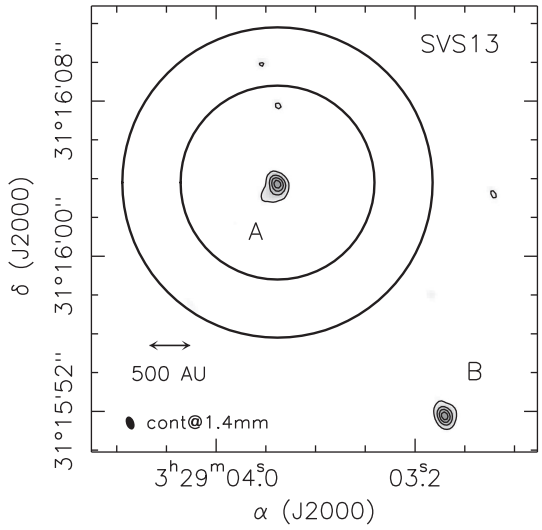

Figure 1. The SVS13 star-forming cluster as observed using continuum emission at 1.4 mm with the PdBI by De Simone et al. (2017). Two objects dominate at mm wavelengths: the Class I system called A and the earlier Class 0 object called B. The solid rings show the HPBWs of the IRAM 30 m for the NO transitions detected at 2 and 1 mm towards SVS13-A.

gas. Finally, in environments dominated by low-velocity shocks (∼20 kms^{-1}) NO seems to also be a direct probe of the molecular oxygen abundance. Indeed, low-velocity shock models indicate that the behaviour of NO is similar to that of O_2 in that they are abundant (and deficient) at similar times (Chen et al. 2014). Since O_2 is not readily observable with ground-based telescopes, NO may prove to be a good proxy for the molecular form of oxygen.

In this paper, we present NO detections towards two objects: the SVS13-A Class I system and the outflow spot L1157-B1. Both environments are warm, but they significantly differ from their chemical composition and past history. These two regions are described in detail in Section 2. In Section 3, we describe the observations. In Section 4, we report the results of our excitation analysis. In Section 5, we derive the observed fractional abundances of NO and we model the chemistry of NO to find the origin of its emission in both objects. We briefly present our conclusions in Section 6.

2 THE SAMPLE

2.1 The Class I SVS13-A object

SVS13-A is a ≃32.5 $L_\odot$ (Tobin et al. 2016) young star located in a young stellar objects cluster in the Perseus NGC1333 cloud (d = 235 pc; Hirota et al. 2008). The region has been extensively investigated in the past (see e.g. Chini et al. 1997; Bachiller et al. 1998; Looney, Mundy & Welch 2000; Chen, Launhardt & Henning 2009; Tobin et al. 2016, and references therein). Fig. 1 reports recent 1.4 mm continuum interferometric observations of SVS13 (De Simone et al. 2017) showing SVS13-A as well as the SVS13-B protostar, which lies out of the region sampled with the present IRAM 30-m observations (see Section 3). SVS13-A is associated (i) with a chemically rich hot corino (Codella et al. 2016; De Simone et al. 2017; Lefèvre et al. 2017), (ii) with an extended outflow (>0.07 pc; Lefloch et al. 1998; Codella, Bachiller & Reipurth 1999), as well as (iii) with the well-known chain of Herbig–Haro (HH) objects 7–11 (Reipurth et al. 1993). In addition, SVS13-A has a low $L_{\rm submm}/L_{\rm bol}$ ratio (∼0.8 per cent) and a high bolometric temperature ($T_{\rm bol}$ ∼ 188 K; Tobin et al. 2016). Although still deeply embedded

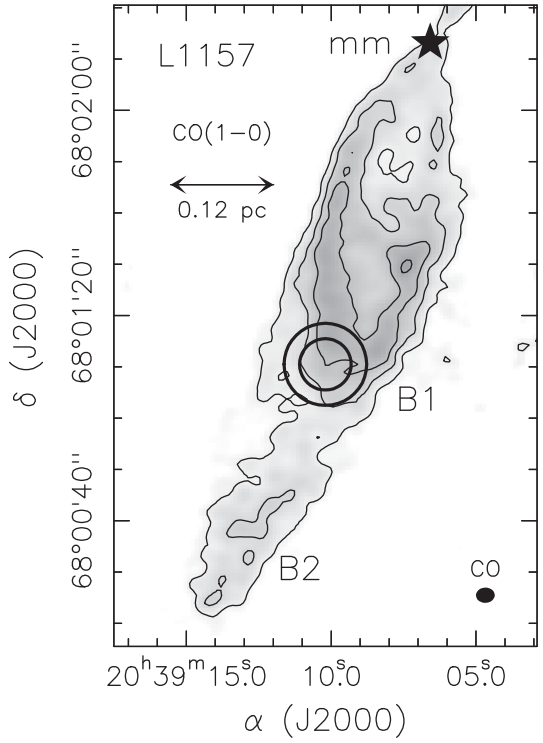

Figure 2. The L1157 southern blueshifted outflow as traced by CO(1–0) emission observed using the IRAM PdB interferometer (Gueth, Guilloteau & Bachiller 1996). The B1 and B2 cavities are labelled. The solid rings show the HPBWs of the IRAM 30 m for the NO transitions detected at 2 and 1 mm towards B1 (see the text). The star marks the position of the L1157-mm protostar.

in a large-scale molecular envelope (Lefloch et al. 1998), SVS13-A is considered a more evolved system, already entered in the Class I evolutionary stage (e.g. Chen, Launhardt & Henning 2009). Finally, we note that VLA observations (e.g. Anglada, Rodríguez & Torrelles 2000; Tobin et al. 2016, and references therein) showed that SVS13-A, once observed at sub-arcsec angular scale, reveals in turn two components (VLA4A and VLA4B) separated by 300 mas, being the hot corino associated only with VLA4B (Lefèvre et al. 2017).

2.2 The L1157-B1 protostellar shock

The L1157-mm Class 0 protostar, located at 250 pc from the Earth (Looney et al. 2007) with a $L_{\rm bol} \simeq 3\ L_\odot$ (Tobin et al. 2010), drives a chemically rich outflow (e.g. Bachiller et al. 2001), associated with molecular clumpy cavities (Gueth, Guilloteau & Bachiller 1996; 1998) that are created by episodic events in a precessing jet (Podio et al. 2016). The brightest shock front is called B1 and is associated with the southern blueshifted outflow lobe (see Fig. 2). The B1 structure has been studied in detail using both single dishes and interferometers, revealing a clumpy bow-like structure, built by several jet-cavity impacts in the last ∼1000 yr, where the abundance of several molecules are enhanced due to a combination of sputtering and warm gas-phase chemistry (e.g. Tafalla & Bachiller 1995; Codella et al. 2009; Benedettini et al. 2013; Busquet et al. 2014; Codella et al. 2015; Lefloch et al. 2017, and references therein).

Table 1. List of NO transitions detected[a] towards SVS13-A and L1157-B1 (see Table 2).

Transition		ν^b	I[b,c]	Source	
$F_u \rightarrow F_l$	$p_u \rightarrow p_l$	(GHz)		SVS13-A	L1157-B1
NO $^2\Pi_{1/2}$ J = 5/2–3/2 (E_u = 19 K)					
7/2 → 5/2	+ → –	250 436.85	99.7	Y	Y
5/2 → 3/2	+ → –	250 440.66	63.1	Y	Y
3/2 → 1/2	+ → –	250 448.53	37.4	Y	Y
5/2 → 5/2	– → +	250 708.25	12.0	N	Y
7/2 → 5/2	– → +	250 796.44	100.0	Y	Y
5/2 → 3/2	– → +	250 815.59	63.3	Y	Y
3/2 → 1/2	– → +	250 816.95	37.6	Y	Y
NO $^2\Pi_{1/2}$ J = 3/2–1/2 (E_u = 7 K)					
5/2 → 3/2	– → +	150 176.48	100.0	Y	Y
3/2 → 1/2	– → +	150 198.76	37.1	N	Y
3/2 → 3/2	– → +	150 218.73	29.6	N	Y
1/2 → 1/2	– → +	150 225.66	29.6	N	Y
3/2 → 3/2	+ → –	150 439.12	29.6	N	Y
5/2 → 3/2	+ → –	150 546.52	100.0	Y	Y
1/2 → 1/2	+ → –	150 580.56	63.3	N	Y
3/2 → 1/2	+ → –	150 644.34	37.6	N	Y

[a]The detected lines have an S/N ratio ≥ 5 and are not contaminated by the emission from other lines (see the text).
[b]From the Cologne Database for Molecular Spectroscopy (CDMS; http://www.astro.uni-koeln.de/cdms/; Müller et al. 2001, 2005) molecular data base.
[c]I is the expected intensity. We assumed I = 100.0 for the brightest component; the intensities of the other hyperfine components are consequently scaled.

3 OBSERVATIONS

The observations of NO were carried out during several runs between 2012 and 2014 with the IRAM 30-m telescope near Pico Veleta (Spain) as part of the Astrochemical Surveys At IRAM[1] (ASAI) Large Programme. Both SVS13-A and L1157-B1 have been observed at 3 mm (80–116 GHz), 2 mm (129–173 GHz), and 1.3 mm (200–276 GHz) using the broad-band EMIR receivers. The observations were acquired towards the following coordinates: SVS13-A: $\alpha_{J2000} = 03^h29^m03^s.3$, $\delta_{J2000} = +31^\circ16'03''.8$; L1157-B1: $\alpha_{J2000} = 20^h39^m10^s.2$, $\delta_{J2000} = +68^\circ01'10''.5$, in wobbler switching mode, with a throw of 180 arcsec.

This studyis based on the NO spectra of the $^2\Pi_{1/2}$ J = 3/2 → 1/2 (at ∼150.2 GHz) and $^2\Pi_{1/2}$ J = 5/2 → 2/2 (at ∼250.8 GHz) transitions (see Table 1). The forward (F_{eff}) and beam efficiencies (B_{eff}) are: 0.93 and 0.72 at 150 GHz, and 0.90 and 0.53 at 251 GHz. We also report emission associated with the $C^{18}O$(2–1) (219 560.350 MHz), $C^{17}O$(2–1) (224 714.190 MHz), $^{13}C^{18}O$(2–1) (209 419.172 MHz), $^{13}C^{17}O$(2–1) (214 573.873 MHz), and CS(5–4) (244 935.560 MHz) transitions detected towards SVS13-A. All the frequency values have been extracted from the Cologne Database for Molecular Spectroscopy (CDMS; Müller et al. 2001, 2005) molecular data base. The pointing was checked by observing nearby planets or continuum sources and was found to be accurate to within 2–3 arcsec. The telescope HPBWs are 16 arcsec at 150.2 GHz and 10 arcsec at 250.8 GHz. The data reduction was performed using the GILDAS-CLASS[2] package. Calibration uncertainties are estimated to be ≃ 20 per cent. Note that the lines observed at 2 mm towards SVS13-A (see Section 4) are affected by emission at OFF position observed in wobbler mode. Line intensities have been converted from antenna temperature to main beam temperature (T_{MB}), using the main beam efficiencies reported in the IRAM 30-m website.[3]

Table 2. Parameters of the hyperfine fits to the observed NO lines (see Table 1).

T_{ex} (K)	rms[a] (mK)	V_{peak} (km s^{-1})	FWHM (km s^{-1})	$\sum_i \tau_i$	N_{tot}[b] (cm^{-2})
SVS13-A					
NO $^2\Pi_{1/2}$ J = 5/2–3/2					
≥4	8	+8.6 ± 0.1)	1.5 ± 0.1	≤0.2	≤3 × 10^{15}
L1157-B1					
NO $^2\Pi_{1/2}$ J = 5/2–3/2					
5 ± 1	7	+0.6 ± 0.1	5.0 ± 0.2	0.6 ± 0.2	5.5 ± 1.5 × 10^{15}
NO $^2\Pi_{1/2}$ J = 3/2–1/2					
≥4	9	+0.6 ± 0.3	4.7 ± 0.2	≤0.2	≤4 × 10^{15}

[a]At a spectral resolution of 0.47 km s^{-1} (SVS13-A), 0.93 km s^{-1} (L1157-B1; $^2\Pi_{1/2}$ J = 5/2–3/2), and 0.78 km s^{-1} (L1157-B1; $^2\Pi_{1/2}$ J = 3/2–1/2).
[b]Assuming LTE and a source size of 26 arcsec (SVS13-A) and 20 arcsec (L1157-B1; see the text).

4 RESULTS

The NO emission due to $^2\Pi_{1/2}$ J = 3/2 → 1/2 and $^2\Pi_{1/2}$ J = 5/2 → 3/2 transitions has been detected towards both the SVS13-A and L1157-B1 sources. In particular, Table 1 reports all the hyperfine components detected above 5σ. Figs 3–6 report the observed spectra, which are discussed below for both sources.

We used the GILDAS-CLASS tool to fit separately the NO $^2\Pi_{1/2}$ J = 3/2 → 1/2 and $^2\Pi_{1/2}$ J = 5/2 → 3/2 spectra (see Table 2), obtaining the best fit of the hyperfine components providing four parameters (see Codella et al. 2012): (i) the LSR velocity, (ii) the linewidth (FWHM), (iii) the sum of the opacity at the central velocities of all the hyperfine components $p_1 = \sum_i \tau_i$, and (iv) the product $p_2 = p_1 \times [J(T_{ex})–J(T_{bg})–J(T_c)]$, where $J(T) = \frac{h\nu/k}{e^{h\nu/kT}-1}$ and T_c is the temperature of the continuum emission, which can be neglected for both sources here analysed (see below). Hence,

$$T_{ex} = \frac{h\nu}{k}\left[\ln\left(1+\frac{h\nu}{k}\frac{p_1}{p_2}\right)\right]^{-1}. \quad (1)$$

The derived T_{ex} depends also on the assumed source extent to reproduce the observed T_{mb} and will be discussed separately for each source.

4.1 SVS13-A

Fig. 3 shows in black the emission lines due to the NO $^2\Pi_{1/2}$ J = 5/2–3/2 hyperfine components observed at ≃250 GHz (Table 1). The HPBW of 10 arcsec ensures no contamination due to the SVS13-B protostar (see Fig. 1). The red line shows the fit obtained with the CLASS tool: the lines are well peaked at the systemic velocity of +8.6 km s^{-1} (Chen, Launhardt & Henning 2009), the FWHM is quite narrow (1.5 ± 0.1 km s^{-1}), and the emission looks optically thin. Note that the F = 5/2–3/2 and 3/2–1/2 (– → +) transitions of the $^2\Pi_{1/2}$ J = 5/2–3/2 pattern are blended at the present observed resolution, as clearly shown in Fig. 3.

[1] www.oan.es/asai
[2] http://www.iram.fr/IRAMFR/GILDAS
[3] http://www.iram.es/IRAMES/mainWiki/Iram30mEfficiencies

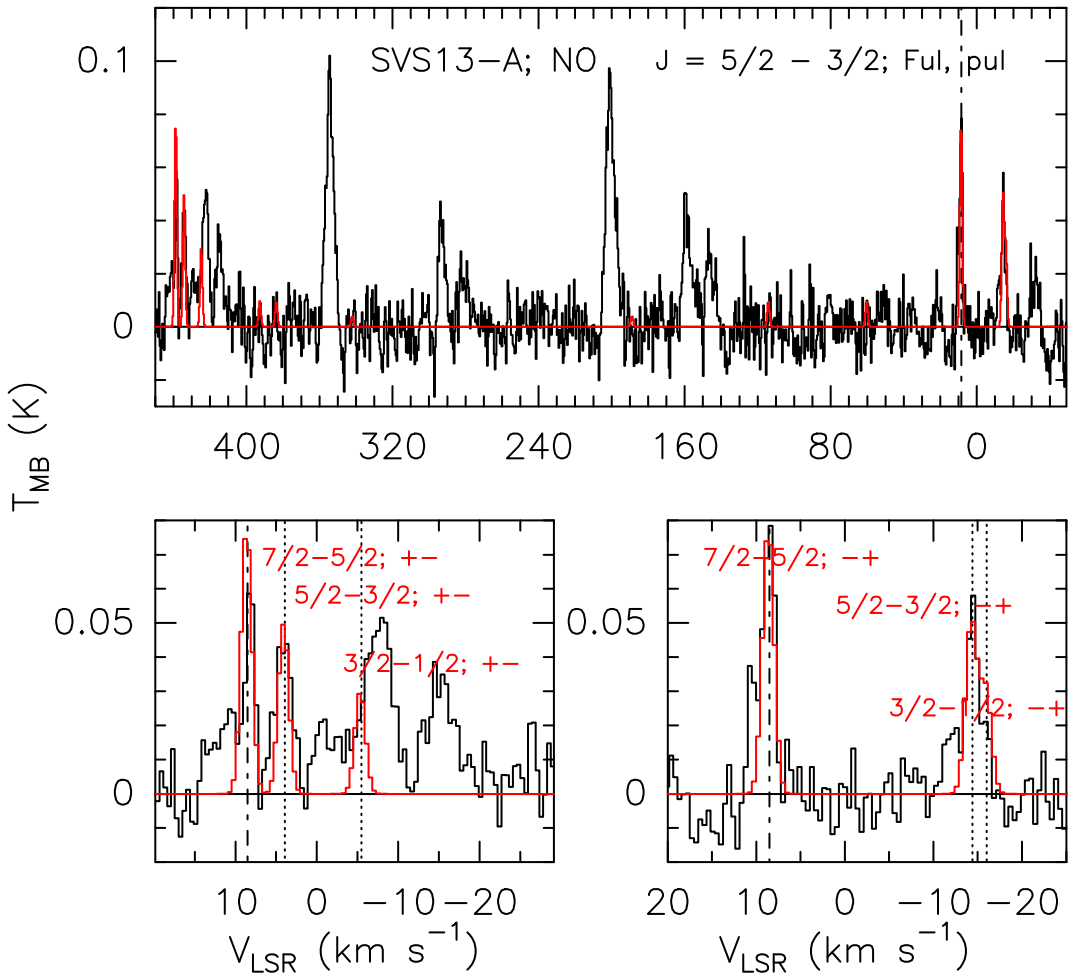

Figure 3. *Upper panel:* emission due to the NO $^2\Pi_{1/2}$ J = 5/2–3/2 spectral pattern (black histogram; see Table 1; in T_{mb} scale after correction for beam dilution, see the text) observed towards SVS13-A with the IRAM 30-m antenna. The red line shows the best fit obtained with the GILDAS-CLASS package using the simultaneous fit of all the hyperfine components (see Table 2). For sake of clarity, the hyperfine components are not indicated in the upper panel and are labelled in the zoom-in in the lower panels. The spectrum is centred at the frequency of the hyperfine component $F_{ul} = 7/2–5/2$; $p_{ul} = + \rightarrow -$ (250 436.85 MHz). The vertical dashed line indicates the ambient LSR velocity (+8.6 km s^{-1}, Chen, Launhardt & Henning 2009). *Bottom-right panel:* zoom-in of the upper panel. Dotted lines indicate the hyperfine components falling in that portion of the spectrum. Note that the $F_{ul} = 3/2–1/2$ $p_{ul} = - \rightarrow +$ line is blended with the brighter $F_{ul} = 5/2–1/2$ $p_{ul} = - \rightarrow +$ one. The analysis of the residual is shown in Fig. 8. *Bottom-left panel:* zoom-in of the upper panel, after having centred the spectrum at the frequency of the hyperfine component $F_{ul} = 7/2–5/2$; $p_{ul} = + \rightarrow -$ (250 796.44 MHz). The $F_{ul} = 3/2–1/2$ $p_{ul} = + \rightarrow -$ line is blended with the $13_{9,4}–12_{9,3}$ intense emission at 250 450.21 MHz due to CH_3CHO-E, a well-known tracer of hot corinos (as that around SVS13-A). For the legibility of the figure, given the complexity of this portion of the spectrum, the residual is not reported.

What is the size of the region emitting in NO? Instructive information comes from the linewidth, which is indeed narrower than that tracing the inner 100 au of the protostellar environment, i.e. the hot corino, which is 4–5 km s^{-1} accordingly to recent single-dish and interferometric observations of SVS13-A (López-Sepulcre et al. 2015; Codella et al. 2016; De Simone et al. 2017). On the other hand, the NO linewidth (1.5 km s^{-1}) is in perfect agreement with that of CS(5–4), a tracer of the molecular envelope (see Table 3 and Fig. 7). Indeed, Lefloch et al. (1998) mapped the SVS13-A region in CS(5–4) using the IRAM 30-m antenna revealing an envelope with size of $\simeq$ 39 arcsec × 17 arcsec ($\simeq$0.04 × 0.02 pc). The temperature has been estimated from continuum to be around 40 K (Lefloch et al. 1998; Chen, Launhardt & Henning 2009). In addition, also the $C^{18}O$ and $C^{17}O$ lines here detected in the context of ASAI (Table 3 and Fig. 7) also show similar FWHM. All these findings support the association of the NO $^2\Pi_{1/2}$ J = 5/2–3/2 emission with the molecular envelope surrounding the SVS13-A protostar. Consequently, we applied no filling factor correction since the envelope size is larger than 17 arcsec. We then derive the excitation temperature T_{ex} by considering the opacity less than 0.2. The continuum emission, roughly estimated from the high-quality baselines obtained by the Wobbler mode observations ($\sim$80 mK in T_{MB} scale), can be neglected. We obtain low T_{ex}, $\geq$ 4 K, clearly indicating that the LTE conditions are not fully satisfied and that the density of the observed envelope has to be less than the critical densities of the observed NO lines, which are, according to the collisional rates with H_2 derived by Lique et al. (2009), $\sim 10^5$ cm^{-3} in the 10–50 K range (see http://home.strw.leidenuniv.nl/ moldata/datafiles/no.dat). In addition, it has to be noted that the low excitation ($E_u < 20$ K) does not make the observed NO lines the best candidates to probe high kinetic temperatures. The total column density of NO is then estimated to be $N(NO) \leq 3 \times 10^{15}$ cm^{-2}.

Interestingly enough, Fig. 8 (bottom and middle panels) shows that if we inspect the best Gaussian fit of the NO $^2\Pi_{1/2}$ J = 5/2–3/2

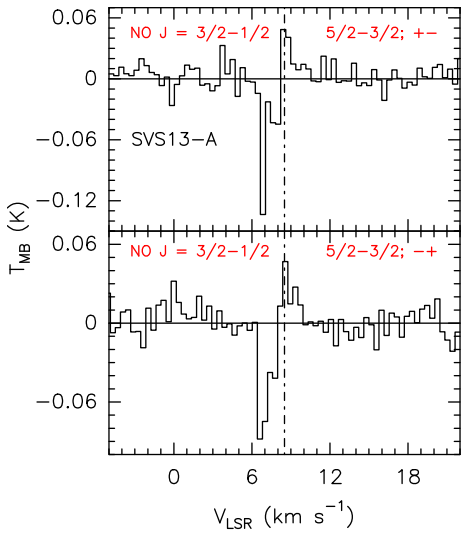

Figure 4. *Upper panel:* spectral signatures due to the NO $^2\Pi_{1/2}$ J = 3/2–1/2 spectral pattern (black histogram; see Table 1; in T_{mb} scale after correction for beam dilution, see the text) observed towards SVS13-A with the IRAM 30-m antenna. The spectrum is centred at the frequency of the hyperfine component F_{ul} = 5/2–3/2; p_{ul} = + → – (150 546.52 MHz). The vertical dashed line indicates the ambient LSR velocity (+8.6 km s^{-1}, Chen, Launhardt & Henning 2009). The absorption is due to emission in the OFF position, observed in wobbler mode with a throw of 180 arcsec (see Section 3). *Bottom panel:* same as for the upper panel for the hyperfine component F_{ul} = 5/2–3/2; p_{ul} = – → + (150 176.48 MHz).

F_{ul} = 7/2–5/2; 5/2–3/2, and 3/2–1/2; p_{ul} = + → – emission (i.e. the more isolated hyperfine components of the J = 5/2–3/2 pattern), we see a non-negligible residual at ∼3σ (see the purple filled histograms). These profiles suggest non-Gaussian emission from gas at blueshifted velocity. Indeed the residual of the C^{18}O(2–1) and C^{17}O(2–1) shows wings (Fig. 8, upper panel) associated with the well-known extended molecular blueshifted and redshifted outflow driven by SVS13-A (e.g. Lefloch et al. 1998). The present NO $^2\Pi_{1/2}$ J = 5/2–3/2 emission thus suggests an outflow component, to be confirmed by higher sensitivity observations. If we conservatively assume an excitation temperature between 5 and 50 K and optically thin emission, we derive a column density N(NO) ∼ 10^{14}–10^{15} cm^{-2} in the wings.

Finally, in addition to the NO emission at ∼250 GHz, Fig. 4 reports the spectral signature of the NO $^2\Pi_{1/2}$ J = 3/2–1/2 spectral pattern observed towards SVS13-A with an HPBW = 16 arcsec. Only the hyperfine component F_{ul} = 5/2–3/2; p_{ul} = + → – (150 546.52 MHz), and F_{ul} = 5/2–3/2; p_{ul} = – → + (150 176.48 MHz) are detected. Both profiles are characterized by a weak emission centred at the systemic velocity of +8.6 km s^{-1}, and are severely contaminated by a deep absorption due to emission in the OFF position, observed in wobbler mode with a throw of 180 arcsec (see Section 3). The absorption is present in the 150 GHz spectrum, taken with a HPBW of 16 arcsec, and not at 251 GHz, where the beam is definitely smaller, i.e. 10 arcsec. However, considered that the 150 and 251 GHz observations have not been observed simultaneously, different locations of the OFF position around the ON source could have played a role. The absorption is blueshifted suggesting contamination due to gas associated with the molecular cloud hosting nearby protostellar systems (e.g. the systemic velocity of the close NGC1333-IRAS4A and -IRAS2A objects is ∼+7.2 km s^{-1}; e.g. Santangelo et al. 2015; De Simone et al. 2017). The poor NO $^2\Pi_{1/2}$ J = 3/2–1/2 spectra prevent us to obtain a reliable fit. However, we verified that what found at ∼150 GHz is consistent with the solution provided by the fit of the $^2\Pi_{1/2}$ J = 5/2–3/2: N(NO) ≤ 3 × 10^{15} cm^{-2}.

4.2 L1157-B1

Figs 5 and 6 show in black the emission lines due to the NO $^2\Pi_{1/2}$ J = 5/2–3/2 and J = 3/2–1/2 hyperfine components, reported in Table 1. The red lines show the fit of the NO hyperfine structure obtained with GILDAS-CLASS: the emission lines of both spectral patterns have FWHMs ≃ 5 km s^{-1} and peak at ∼+0.6 km s^{-1}, being blueshifted by about 2 km s^{-1} (V_{LSR} = +2.6 km s^{-1}; Bachiller et al. 2001). Note that the brightest lines show blue wings (in addition to the Gaussian profile; see also the residuals in Figs 5 and 6) with velocities up to ∼8 km s^{-1} from the systemic velocity. As for SVS13-A, the F = 5/2–3/2 and 3/2–1/2 (– → +) transitions of the $^2\Pi_{1/2}$ J = 5/2–3/2 pattern are blended at the present observed resolution (see Fig. 5). We thus report for the first time the association of NO emission with a shocked region driven by a low-mass protostar. Lefloch et al. (2012) showed that several components of L1157-B1 can be disentangled through the analysis of molecular line profiles, namely: (i) the compact (≥10 arcsec) gas associated with the impact between the precessing jet and the cavities, dominating at velocities less than –20 km s^{-1}; (ii) the extended (20 arcsec) B1 cavity (≃1100 yr old; Podio et al. 2016), dominating at velocities between about −20 and −5 km s^{-1}; (iii) the older extended (again ∼20 arcsec) cavity remnant associated with the B2 jet episode, dominating at velocities close to the systemic one. The velocity range of the NO emission is in good agreement with that of several molecular species (such as CS, H_2CO, NH_3; see Bachiller et al. 2001; Codella et al. 2010; Benedettini et al. 2013; Gómez-Ruiz et al. 2015) tracing the extended B1 and B2 cavities, outlined in Fig. 2 and encompassed by both the HPBWs of the present observations. This will allow us to assume for the NO emission in L1157-B1 an emitting size of 20 arcsec (the typical size of both the B1 and B2 emission) and consequently to apply the filling factor correction.

To derive the excitation temperature T_{ex}, the contribution due to continuum can be neglected, given that no continuum emission has been so far detected towards L1157-B1 (e.g. Codella et al. 2015, and references therein). Once taken into account the opacities derived from the Gaussian fit (opacity less than 0.6), we consistently derive for both the NO spectral patterns observed at ∼150 and ∼250 GHz an excitation temperature T_{ex} ≃ 5 K. Also in this case, the low T_{ex} values suggest that the gas is not fully in LTE conditions. As reported before, the critical densities of the observed NO lines at 250 GHz are ∼10^5 cm^{-3} (Lique et al. 2009). On the other hand, the critical densities of the transitions at 150 GHz, in the 10–50 K range, are ∼10^4 cm^{-3}. These values are similar to the minimum density derived by Gómez-Ruiz et al. (2015) from CS for the extended old (∼2000 yr) cavity (5 × 10^4 cm^{-3}). Considered the measure of T_{ex} and the corresponding error, the total NO column density is N(NO) = 5.5 ± 1.5 × 10^{15} cm^{-2}.

5 DISCUSSION

5.1 Abundances

To estimate the NO abundance (X_{NO}) in the SVS13-A envelope, we evaluated the H_2 column density using the emission from the J = 2–1 transition of several CO isotopologues (Table 3): C^{18}O, C^{17}O, and ^{13}C^{18}O, expected to be optically thin. We also detect ^{13}C^{17}O(2–1) emission with a signal-to-Noise (S/N) ratio ∼ 3–4.

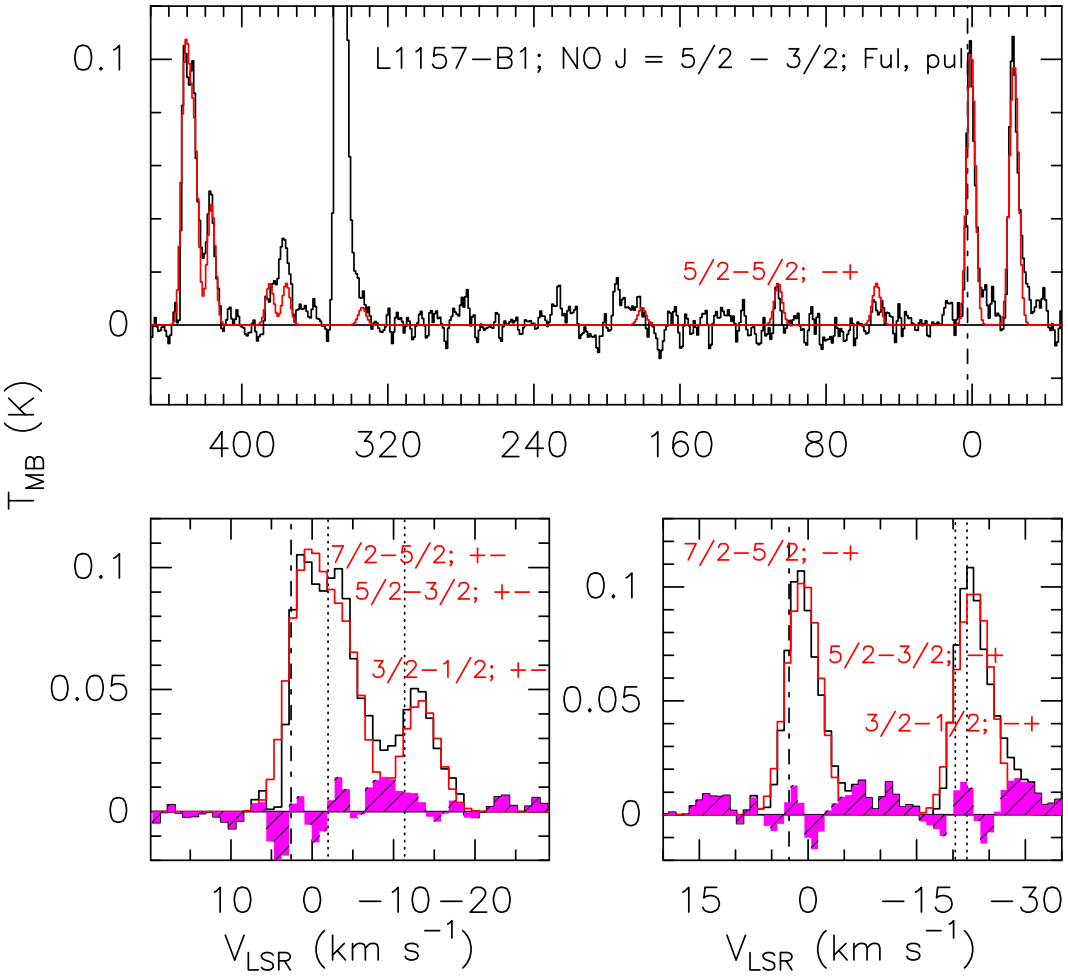

Figure 5. *Upper panel:* emission due to the NO $^2\Pi_{1/2}$ J = 5/2–3/2 spectral pattern (black histogram; see Table 1; in T_{mb} scale observed towards L1157-B1 with the IRAM 30-m antenna. The red line shows the best fit obtained with the GILDAS-CLASS package using the simultaneous fit of all the hyperfine components (see Table 2). For sake of clarity, the hyperfine components that are not indicated in the upper panel are labelled in the zoom-in in the lower panels. The spectrum is centred at the frequency of the hyperfine component F_{ul} = 7/2–5/2; p_{ul} = + → – (250 436.85 MHz). The vertical dashed line indicates the ambient LSR velocity (+2.6 km s^{-1}; Bachiller et al. 2001). *Bottom-right panel:* zoom-in of the upper panel. Dotted lines indicate the hyperfine components falling in that portion of the spectrum. Note that the F_{ul} = 3/2–1/2 p_{ul} = – → + line is blended with the brighter F_{ul} = 5/2–1/2 p_{ul} = – → + one. The purple filled histogram shows the residual after Gaussian fit (red) of the NO emission (black). *Bottom-left panel:* zoom-in of the upper panel, after having centred the spectrum at the frequency of the hyperfine component F_{ul} = 7/2–5/2; p_{ul} = + → – (250 796.44 MHz).

All these lines have been observed with the same HPBWs (10–12 arcsec) and show FWHMs consistent with that of the NO profiles (Table 3), indicating that the rare CO isotopologues are reasonably tracing the same material, i.e. the molecular envelope. Adopting local thermodynamic equilibrium (LTE) conditions, optically thin emission, and assuming a kinetic temperature of 40 K (Lefloch et al. 1998), [^{16}O]/[^{18}C]=560, [^{18}O]/[^{17}C] = 3, [^{12}C]/[^{13}C] = 77, and [^{12}CO]/[H_2] = 10^{-4} (Wilson & Rood 1994), we derive N(CO) = 3–10 × 10^{18} cm^{-2}. Consequently, X_{NO} towards SVS13-A is ≤3 × 10^{-7}. Interestingly, if we use the tentative NO detection towards the SVS13-A low-velocity outflow and the C^{17}O emission at the same velocities (see Fig. 8) we obtain an NO abundance of 0.1–5 × 10^{-7} i.e. a value equal or slightly higher than that in the SVS13-A envelope.

For the L1157-B1 analysis, we can use the source-averaged column density N(CO) = 1 × 10^{17} cm^{-2}, found for both the B1 and B2 cavities by Lefloch et al. (2012). We can thus derive the NO abundance towards a shocked region: X(NO) = 4–7 × 10^{-6}. To our knowledge, there are few measurements of the NO abundances in low-mass star-forming regions. Yıldız et al. (2013) reported X(NO) = 2 × 10^{-8} towards the NGC1333-IRAS4A star-forming region, suggesting NO is tracing an extended photodissociation region (PDR) outside the protostellar core. Similar abundances (1–3 × 10^{-8}) have been reported for starless cores such as e.g. L1544 (Akylmaz et al. 2007). The high abundance derived for L1157-B1 as well as that tentatively derived for the SVS13-A outflow (few 10^{-7}) supports a large increase of the NO production, either due to direct release from dust mantles and/or by warm gas-phase chemistry. In the following, we make use of the public code UCLCHEM (Holdship et al. 2017) to investigate the origin of the NO emission in each object. The code is fully described in Holdship et al. (2017) and references therein. Briefly, the code computes the fractional abundances of gas and solid species as a function of time. Beside the standard chemical gas-phase reactions, freeze out, non-thermal (due to UV radiation and cosmic rays), thermal desorption, and a basic network of surface reactions are all included.

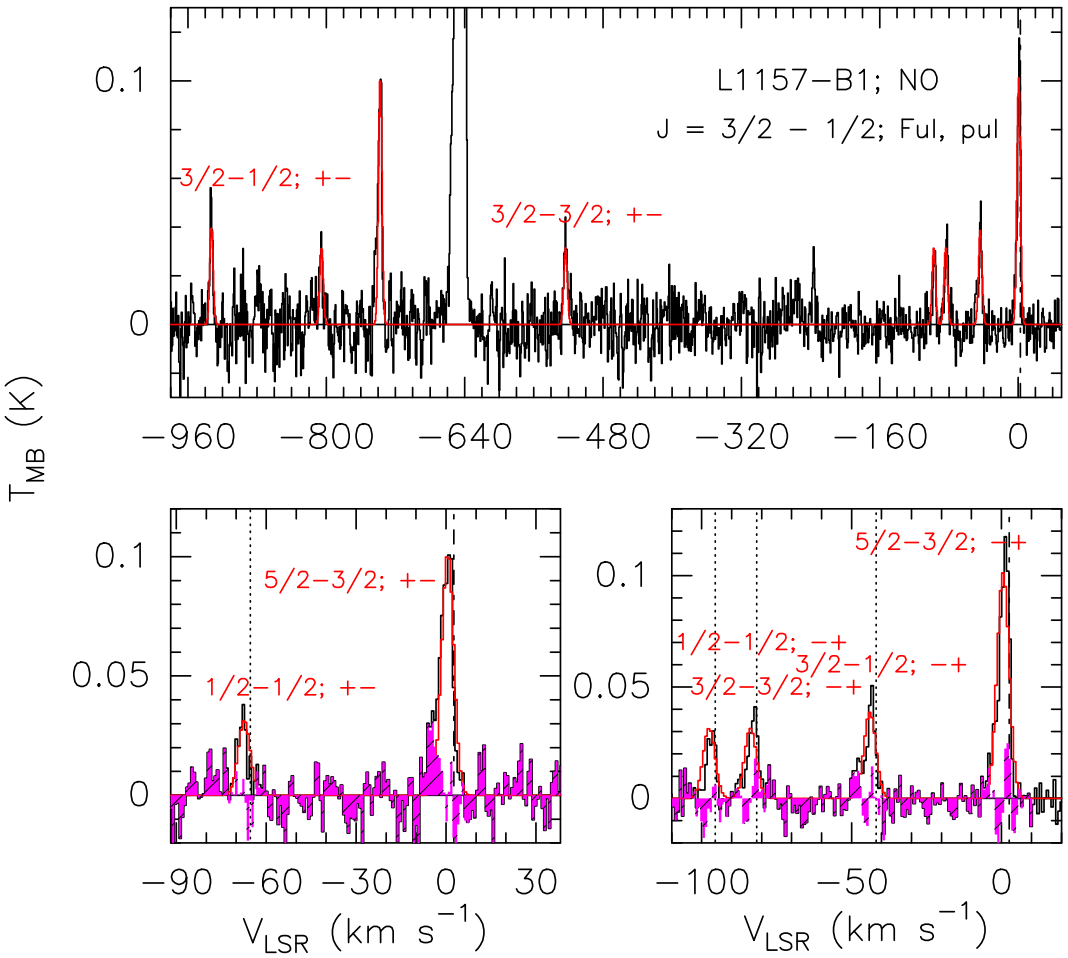

Figure 6. *Upper panel:* emission due to the NO $^2\Pi_{1/2}$ J = 3/2–1/2 spectral pattern (black histogram; see Table 1; in T_{mb} scale after correction for beam dilution, see the text) observed towards L1157-B1 with the IRAM 30-m antenna. The red line shows the best fit obtained with the GILDAS–CLASS package using the simultaneous fit of all the hyperfine components (see Table 2). For sake of clarity, the hyperfine components that are not indicated in the upper panel are labelled in the zoom-in in the lower panels. The spectrum is centred at the frequency of the hyperfine component $F_{ul} = 5/2–3/2$; $p_{ul} = - \rightarrow +$ (150 176.48 MHz). The vertical dashed line indicates the ambient LSR velocity (+2.6 km s^{-1}; Bachiller et al. 2001). *Bottom-right panel:* zoom-in of the upper panel. Dotted lines point the hyperfine components falling in that portion of the spectrum. The purple filled histogram shows the residual after Gaussian fit (red) of the NO emission (black). *Bottom-left panel:* zoom-in of the upper panel, after having centred the spectrum at the frequency of the hyperfine component $F_{ul} = 5/2–3/2$; $p_{ul} = + \rightarrow -$ (150 546.52 MHz).

Table 3. List of CO and CS transitions and line properties (in T_{MB} scale) detected towards SVS13-A and used in the present analysis.

Transition	ν^a (MHz)	E_u (K)	*HPBW* (arcsec)	*Dv* (km s^{-1})	rms (mK)	$T_{peak}{}^b$ (mK)	$V_{peak}{}^b$ (km s^{-1})	FWHM^b (km s^{-1})	$I_{int}{}^b$ (mK km s^{-1})
$^{13}C^{18}O$(2–1)	209 419.172	15	12	0.56	9	129 ± 13	+8.4 ± 0.1	1.5 ± 0.2	78 ± 1
$^{13}C^{17}O$(2–1)	214 573.873	15	12	0.55	10	18 ± 3	+8.2 ± 0.4	1.7 ± 0.9	32 ± 15
$C^{18}O$(2–1)	219 560.350	16	11	0.53	53	5370 ± 150	+8.6 ± 0.1	1.6 ± 0.1	8873 ± 74
$C^{17}O$(2–1)	224 714.190	16	11	0.52	18	1068 ± 69	+8.2 ± 0.1	2.0 ± 0.1	2315 ± 28
CS(5–4)	244 935.560	35	10	0.49	20	386 ± 71	+8.3 ± 0.1	1.4 ± 0.1	592 ± 26

[a]From the Cologne Database for Molecular Spectroscopy (CDMS; http://www.astro.uni-koeln.de/cdms/). Müller et al. 2001, 2005) molecular data base.
[b]The errors are the Gaussian fit uncertainties (1σ) and are in units of the last digit.

5.2 Chemical modelling of SVS13-A

In the previous section, we established that NO is almost certainly arising from the molecular envelope surrounding the SVS13-A protostar. In order to simulate the envelope, we run UCLCHEM in two Phases: in Phase 1, we start from a purely atomic gas at low density ($n_H = 10^2$ cm^{-3}), and allow the gas to collapse in free-fall until a gas density of 10^4 is reached (the gas density estimated in Section 4.1). The time it takes to reach this density is of course the free-fall timescale, which is $\sim 5 \times 10^6$ yr. This Phase is then either stopped, or allowed to continue for a further 5 million years (assuming a typical lifetime for the parent molecular cloud of $\sim$10 Myr; Mouschovias,

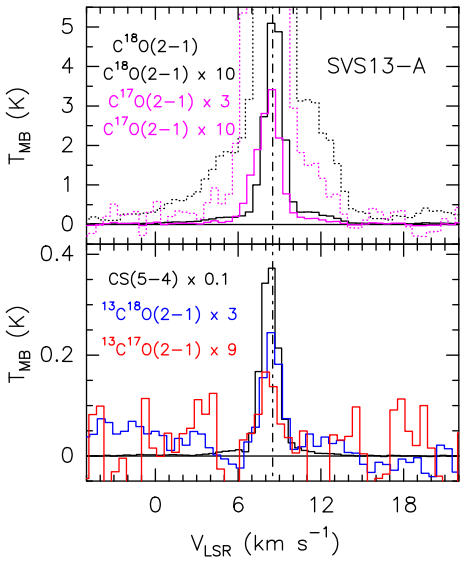

Figure 7. Emission detected towards SVS13-A with the IRAM 30 m in the 1 mm spectral window with HPBWs consistent with that used for the observations of NO $^2\Pi_{1/2}$ J = 5/2–3/2. *Upper panel:* $C^{18}O$(2–1) and $C^{17}O$(2–1) lines (in T_{mb} scale; also increased by different factors to show the outflow wings; dotted histograms). The vertical dashed line indicates the ambient LSR velocity (+8.6 km s^{-1}; Chen, Launhardt & Henning 2009). *Bottom panel:* $^{13}C^{18}O$(2–1), $^{13}C^{17}O$(2–1), and CS(5–4) profiles, scaled to be drawn on the same scale.

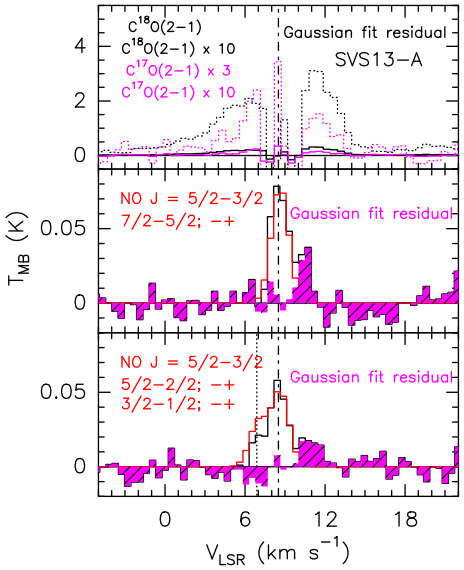

Figure 8. *Upper panel:* residual of the $C^{18}O$(2–1) and $C^{17}O$(2–1) emission after Gaussian fit, showing the outflow wings. The vertical dashed line indicates the ambient LSR velocity (+8.6 km s^{-1}; Chen, Launhardt & Henning 2009). *Middle and bottom panel:* the purple filled histogram shows the residual after Gaussian fit (red) of the NO $^2\Pi_{1/2}$ J = 5/2–3/2 F_{ul} = 7/2–5/2; 5/2–3/2, and 3/2–1/2; p_{ul} = + → – emission (black).

Tassis & Kunz 2006). We adopt the solar initial elemental abundances reported by Asplund et al. (2009, see Table 4).

Phase 2, which starts at a density determined by the final step of Phase 1, then follows the chemical evolution as a function of time at constant density but at a temperature of 40 K, as assumed in the previous sections and also in agreement with Lefloch et al. (1998). In Fig. 9, we show our results for Phase 2, following a Phase

Table 4. List of initial elemental fractional abundances (with respect to the total number of hydrogen nuclei) for Phase I of UCLCHEM, taken from Asplund et al. (2009).

Species	Injected (/H)
He	0.085
O	4.898×10^{-4}
C	2.692×10^{-4}
N	6.761×10^{-5}
S	1.318×10^{-5}
Mg	3.981×10^{-5}
Si	3.236×10^{-5}
Cl	3.162×10^{-7}
P	2.57×10^{-9}
F	3.6×10^{-8}

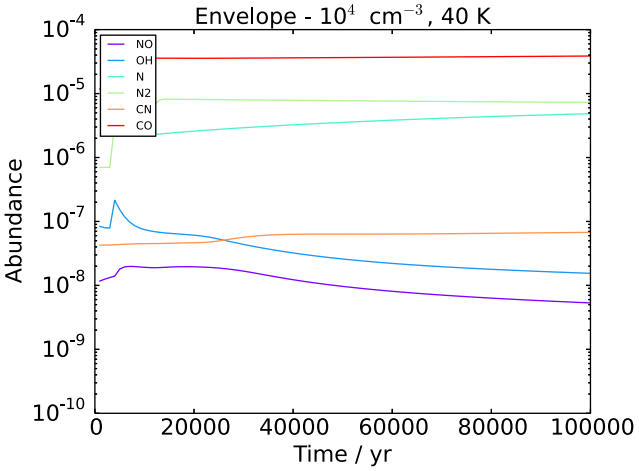

Figure 9. Theoretical fractional abundances of NO, OH, and other selected species as a function of time, for Phase 2, for the envelope of SVS13-A for our best matching model, assuming a density of 10^4 cm^{-3} and a kinetic temperature of 40 K (see the text).

1 of 10 Myr, for an envelope at 10^4 cm^{-3}: NO steadily decreases with time and its abundance always remains below 10^{-8} for times $>2 \times 10^4$ yr, in agreement with the derived 10^{-7} upper limit. NO here forms via the neutral–neutral reaction of N + OH, and its behaviour indeed follows closely that of OH which steadily decreases to form CO. We conclude that the observed NO can indeed be explained by the presence of an envelope with a likely gas density of $\sim 10^4$ cm^{-3}.

Since we encompass the hot corino as well as the envelope of this protostar within our beam, it is important to verify whether a contribution from the hot corino should have been present. In order to model the hot corino, we run UCLCHEM again in two phases; like before, in Phase 1 we start from a purely atomic gas at low density, and allow the gas to collapse in free-fall until a gas density of either 10^7 cm^{-3} or 10^8 cm^{-3} is reached. In Phase 2, the dense gas is 'placed' at a distance of ∼10 au from the star and we allow the temperature to increase up to a value of 80–100 K. The increase in temperature with time is set up in a similar manner to the 1 $M_\odot$ model by Awad, Viti & Williams (2010), but with the assumption that the final mass of the star is 0.75 $M_\odot$, as determined from the 1.4 mm dust continuum observations of Chen, Launhardt & Henning (2009). As the temperature increases, the mantle sublimates in various temperature bands (see Collings et al. 2004).

Phase 2 follows the gas and mantle chemical evolution with time up to 10^5 yr, a reasonable age of a protostar entering the Class I stage. In order to exclude a contribution from the hot corino, the NO fractional abundance with respect to the total number of hydrogen nuclei ought to be less than 3×10^{-7}. This is in fact the case up to $>9 \times 10^4$ yr. While we do not have such as accurate age for the Class I protostar, it is likely that its age does not exceed this value. In addition, note that beams of 10–16 arcsec, as those used to observe the present NO emission imply severe beam dilution for an emitting size of 1 arcsec (typical of hot corinos such as the SVS13-A one; see De Simone et al. 2017; Lefèvre et al. 2017). In particular, the filling factor is equal to 4×10^{-3} (16 arcsec) and 10^{-2} (10 arcsec).

In conclusion, the present data set confirm that high-sensitivity observations allow one to reveal molecules (such as NO), whose emission can challenge the models so far used for protostellar systems. Indeed high-angular interferometric observations of NO emission are clearly needed to provide a comprehensive picture of the SVS13-A system.

5.3 Chemical modelling of L1157-B1

UCLCHEM has been used to model the molecular emission from this object, as well as other shocked spots in low-mass outflow, in several studies (Viti et al. 2011; Gómez-Ruiz et al. 2016; Holdship et al. 2017). For L1157-B1, the best-fitting models have so far indicated a shock velocity ranging from 20 to 40 km s^{-1} and a pre-shock density of at least 10^4 cm^{-3}.

For this work, we used the grid of models already ran in Holdship et al. (2017). In summary, the grid covers pre-shock densities conservatively ranging from 10^3 to 10^5 cm^{-3}, and shock velocities from 10 to 65 km s^{-1} (see their table 2). In fact, based on previous work, we shall exclude from our discussion all models with a pre-shock density of 10^3 cm^{-3}; this is further justified by our excitation analysis in the previous section which implies a gas density of at least 10^4 cm^{-3} (we note that even a pre-shock density of 10^3 cm^{-3} implies a post-shock density of $\sim 4 \times 10^3$ cm^{-3}, still lower than the density inferred from our excitation analysis of 10^4 cm^{-3}). We then find that the models which achieve a high enough abundance of NO to match the observations are: (i) either those with a pre-shock density of 10^5 and 10^6 cm^{-3} with, respectively, 45 and 40 kms^{-1} shock velocities, or (ii) models with a pre-shock density of 10^4 cm^{-3} but with a shock velocity of at least 60 kms^{-1}. These two sets of models have in common the maximum temperature the gas attains during the passage of the shock. While we cannot completely exclude a pre-shock density of 10^4 cm^{-3}, we note that such a low pre-shock density requires a very fast shock, which is inconsistent with previous findings. Moreover, the observed abundance for this model is reached for an age larger than 1000 yr. A pre-shock density of 10^5 cm^{-3} with a velocity of 45 km s^{-1} (see Fig. 10), on the other hand, leads to an abundances of $\sim 10^{-6}$ after a few hundred years, consistent with the dynamical time-scales derived by Podio et al. (2016). The increase in NO abundance at $\sim$150 yr is due to the reaction of nitrogen with OH: the latter is enhanced with time due to the reaction of free oxygen with H_2. At later times, NO is more efficiently destroyed by the reaction with free nitrogen, which becomes more abundant when NH_3 starts decreasing (Viti et al. 2011). We note that the NO abundance is maintained through the dissipation length (see Fig. 10) but that, unlike the low-velocity shock model presented in Chen et al. (2014), NO does *not* trace O_2. Clearly there must be a parameter space that one must explore when performing shock modelling, where NO may be a good tracer of molecular oxygen. This model would also be consistent with the best matching models we found for the NH_3, H_2O (Viti et. al. 2011), H_2S (Holdship et al. 2017), and phosphorous-bearing species (Lefloch et al. 2016).

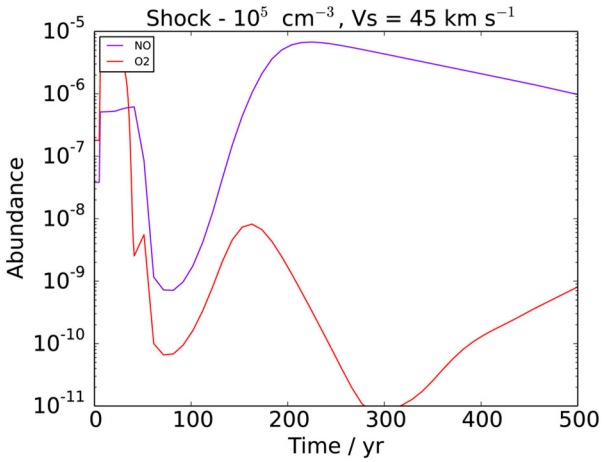

Figure 10. Phase 2 theoretical fractional abundances of NO (blue) and O_2 (red) for our best matching shock model up to the dissipation length, with a pre-shock density of 10^5 cm^{-3} and a shock velocity of 45 km s^{-1}. The kinetic temperature of the pre-shock gas (Phase 1) is 10 K, while the post-shock gas kinetic temperature is 80 K (Tafalla & Bachiller 1995).

6 CONCLUSIONS

The high-sensitivity of the IRAM 30-m ASAI unbiased spectral survey in the mm window allows us to detect, towards the Class I object SVS13-A and the protostellar outflow shock L1157-B1, a large number of NO emission lines, namely the hyperfine components of the $^2\Pi_{1/2}$ J = 3/2 → 1/2 (at 151 GHz) and $^2\Pi_{1/2}$ $J = 5/2 \rightarrow$ 3/2 (at 250 GHz) spectral pattern. The main results of the analysis can be summarized as follows.

(i) Towards the SVS13-A system, narrow (1.5 km s^{-1}), optically thin ($\tau \leq 0.2$) lines peaking at the systemic velocity of +8.6 km s^{-1} have been detected. These findings, also supported by new CS(5–4), $C^{18}O$, $^{13}C^{18}O$, $C^{17}O$, and $^{13}C^{17}O$ lines suggest the association of NO with the molecular envelope with size of $\simeq$20 arcsec (4700 au) surrounding the SVS13-A protostar. The inferred excitation temperature T_{ex} is $\geq$4 K and the total column density N(NO) $\leq 3 \times 10^{14}$ cm^{-2}.

(ii) We observed NO emission towards L1157-B1: the lines are broad (FWHM $\simeq$ 5 km s^{-1}) and blueshifted by about 2 km s^{-1}, thus revealing for the first time NO towards a shocked region driven by a low-mass protostar. The line profiles confirm that NO is associated with the extended (around 20 arcsec) cavity opened by the passage of the jet. We derive $T_{ex} \simeq 5$ K and $N(\mathrm{NO}) = 4\text{–}7 \times 10^{15}$ cm^{-2}.

(iii) We derive a low NO fractional abundance of $\leq 3 \times 10^{-7}$ for the SVS13-A envelope, while a definite X(NO) increase is observed towards the L1157-B1 shock: $4\text{–}7 \times 10^{-6}$. To our knowledge, only few measurements of NO abundances towards low-mass protostellar regions have been so far reported, both around 10^{-8} (extended PDR region around IRAS4A, Yıldız et al. 2013, and starless cores, Akylmaz et al. 2007). The present measurements towards L1157-B1 support a huge increase of the NO production in shocks.

(iv) The public code UCLCHEM has been used to interpret the present NO observations. We confirm that the abundance observed in SVS13-A can be attained by an envelope with a gas density of 10^5 cm^{-3} and a kinetic temperature of 40 K. The NO abundance

in L1157-B1 can be matched by a gas with a pre-shock density of 10^5 cm^{-3} subjected to a shock with velocity of 40–45 kms^{-1}, in agreement with previous findings.

ACKNOWLEDGEMENTS

The authors are grateful to the IRAM staff for its help in the calibration of the 30-m data. We also thank the anonymous referee for instructive comments and suggestions. The research leading to these results has received funding from the European Commission Seventh Framework Programme (FP/2007-2013) under grant agreement No. 283393 (RadioNet3). This work was partly supported by the Italian Ministero dell'Istruzione, Università e Ricerca through the grant Progetti Premiali 2012 – iALMA which is also founding the EB PhD project. This work was supported by the CNRS programme 'Physique et Chimie du Milieu Interstellaire' (PCMI) and by a grant from LabeX Osug@2020 (Investissements davenir - ANR10LABX56). CF aknowledges support from the Italian Ministry of Education, Universities and Research, project SIR (RBSI14ZRHR). JH is funded by an STFC studentship (ST/M503873/1). IJS acknowledges the financial support received from the STFC through an Ernest Rutherford Fellowship (proposal number ST/L004801). BL and CCe acknowledge the financial support from the French Space Agency CNES, and MT and RB from Spanish MINECO (through project AYA2016-79006-P).

REFERENCES

Akyilmaz M., Flower D. R., Hily-Blant P., Pineau des Forêts G., Walmsley C. M., 2007, A&A, 462, 221
Anglada G., Rodríguez L. F., Torrelles J. M., 2000, ApJ, 542, L123
Asplund M., Grevesse N., Sauval A. J., Scott, P, 2009, ARA&A, 47, 481
Awad Z., Viti S., Collings M. P., Williams D. A., 2010, MNRAS, 407, 2511
Awad Z., Viti S., Williams D. A., 2016, ApJ, 826, 207
Bachiller R., Guilloteau S., Gueth F., Tafalla M., Dutrey A., Codella C., Castets A., 1998, A&A, 339, L49
Bachiller R., Peréz Gutiérrez M., Kumar M. S. N., Tafalla M., 2001, A&A, 372, 899
Benedettini M. et al., 2013, MNRAS, 436, 179
Blake G. A., Masson C. R., Phillips T. G., Sutton E. C., 1986, ApJS, 60, 357
Busquet G. et al., 2014, A&A, 561, 120
Chen X., Launhardt R., Henning T., 2009, ApJ, 691, 1729
Chen J-H. et al., 2014, ApJ, 793, 111
Chini R., Reipurth B., Sievers A., Ward-Thompson D., Haslam C. G. T., Kreysa E., Lemke R., 1997, A&A, 325, 542
Codella C., Bachiller R., Reipurth B., 1999, A&A, 343, 585
Codella C. et al., 2010, A&A, 518, L112
Codella C. et al., 2012, ApJ, 744, 164
Codella C., Fontani F., Ceccarelli C., Podio L., Viti S., Bachiller R., Benedettini M., Lefloch B., 2015, MNRAS, 449, L11
Codella C. et al., 2016, MNRAS, 462, L75
Collings M. P., Anderson M. A., Chen R., Dever J. W., Viti S., Williams D. A., McCoustra M. R. S., 2004, MNRAS, 354, 1133
De Simone M. et al., 2017, A&A, 599, 121
Flower D. R., Pineau des Forêts G., Walmsley C. M., 2006, A&A, 456, 215
Gerin M., Viala Y., Pauzat F., Ellinger Y., 1992, A&A, 266, 463
Gerin M., Viala Y., Casoli F., 1993, A&A, 268, 212
Gómez-Ruiz A. I. et al., 2015, MNRAS, 446, 3346
Gómez-Ruiz A. I. et al., 2016, MNRAS, 462, 2203
Gueth F., Guilloteau S., Bachiller R., 1996, A&A, 307, 891
Gueth F., Guilloteau S., Bachiller R., 1998, A&A, 333, 287
Halfen D. T., Apponi A. J., Ziurys L. M., 2001, ApJ, 561, 244
Hily-Blant P., Walmsley C. M., Pineau des Forêts G., Flower D., 2010, A&A, 513, 41
Hirota T. et al., 2008, PASJ, 60, 37
Holdship J., Viti S., Jiménez-Serra I., Priestley F., 2017, ApJ, submitted
Lefèvre C. et al., 2017, A&A, 640, L1
Lefloch B., Castets A., Cernicharo J., Langer W. D., Zylka R., 1998, A&A, 334, 269
Lefloch B. et al., 2012, ApJ, 757, L25
Lefloch B. et al., 2016, MNRAS, 462, 3937
Lefloch B., Ceccarelli C., Codella C., Codella C., Favre C., Podio L., Vastel C., Viti S., Bachiller R., 2017, MNRAS, 469, L73
Lique F., van der Tak F. F. S., Klos J., Balthuis J., Alexander M., 2009, A&A, 493, 557
Liszt H. S., Turner B. E., 1978, ApJ, 224, 73
Looney L. W., Mundy L. G., Welch W. J., 2000, ApJ, 529, 477
Looney L. W., Tobin J. J., Kwon W., 2007, ApJ, 2007, 670, L131
López-Sepulcre A. et al., 2015, MNRAS, 449, 2438
Martín S., Mauersberger R., Martín-Pintado J., García-Burillo S., Henkel C., 2003, A&A, 411, 465
Mouschovias T. C., Tassis K., Kunz M. W., 2006, ApJ, 646, 1043
Müller H. S. P., Thorwirth S., Roth D. A., Winnewisser G., 2001, A&A, 370, L49
Müller H. S. P., Schlöder F., Stutzki J., Winnewisser G., 2005, J. Mol. Struct., 742, 215
Nummelin A., Bergman P., Hjalmarson Å., Friberg P., Irvine W. M., Millar T. J., Ohishi M., Saito S., 2000, ApJS, 128, 213
Podio L. et al., 2016, A&A, 593, L4
Santangelo G. et al., 2015, A&A, 584, A126
Tafalla M., Bachiller R., 1995, ApJ, 443, L37
Tobin J. J., Hartmann L., Looney L. W., Chiang H.-F., 2010, ApJ, 712, 1010
Tobin J. J. et al., 2016, ApJ, 818, 73
Velilla Prieto L. et al., 2015, A&A, 575, 84
Viti S., Collings M. P., Dever J. W., McCoustra M. R. S., Williams D. A., 2004, MNRAS, 354, 1141
Viti S., Jiménez-Serra I., Yates J. A., Codella C., Vasta M., Caselli P., Lefloch B., Ceccarelli C., 2011, ApJ, 740, 3
Wilson T. L., Rood R., 1994, ARA&A, 32, 191
Yıldız U. A. et al., 2013, A&A, 558, A58

This paper has been typeset from a TEX/LATEX file prepared by the author.